Proceedings of the 2010 IEEE
International Conference on Information and Automation
June 20 - 23, Harbin, China

Impedance Analysis for Piezoelectric Energy Harvesting Devices under Displacement and Force Excitations

Junrui Liang and Wei-Hsin Liao
Department of Mechanical and Automation Engineering
The Chinese University of Hong Kong
Shatin, N. T., Hong Kong, China
{jrliang & whliao}@cuhk.edu.hk

***Abstract* - To harvest energy from mechanical vibration with piezoelectric materials, different installations might be adopted according to the vibration conditions of the substrate structures. Surface mount (deformation preferred) and base excitation (movement preferred) are two of the commonly utilized installations. These configurations can be modeled as a general piezoelectric energy harvesting (PEH) device under displacement and force excitations, respectively. Comparison on the dynamics as well as power generation for PEH devices with a real harvesting interface circuit under these two excitations was not made in the previous literatures, since they oversimplified either the mechanical or electrical part. Yet, based on the equivalent impedance network of a general PEH device, the overall dynamics can be investigated. In this paper, the impedance technique is utilized to analyze a PEH device under either excitation condition. Three of the commonly studied interface circuits, including standard energy harvesting (SEH), parallel synchronized switching harvesting on inductor (P-SSHI), and series synchronized switching harvesting on inductor (S-SSHI), are connected in turn as the interface circuit, so as to provide more insights on the harvesting performances of different harvesting devices under different excitations.**

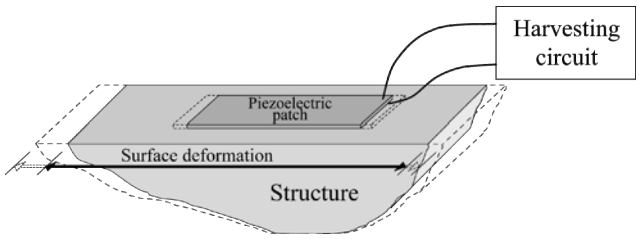

Fig. 1. A surface mount PEH device.

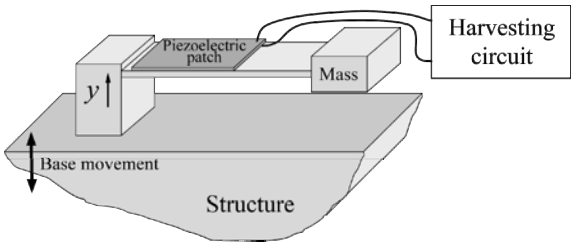

Fig. 2. A base excited PEH device.

I. Introduction

Ambient energy harvesting provides the possibility that ambient energy in different forms (e.g., solar, thermal, wind, vibration) is converted (usually into electrical energy), captured and stored. Wireless sensor networks (WSNs) and mobile electronics are two potential applications for these techniques [1]. During the last few years, accompanying with the development on low power integrated circuits (ICs) and distributed WSNs, researchers investigated how to better harvest the ambient energy.

Mechanical movement or mechanical vibration can be found everywhere in our daily life. It is one of the promising ambient sources to be exploited [2]. Piezoelectric materials, as one of the important and commonly used electromechanical transducers, can be utilized to harvest energy from mechanical vibration sources. In terms of the complexity of the mechanical part, the piezoelectric energy harvesting (PEH) device is the simplest compared to the electromagnetic and electrostatic ones; therefore, it would be more suitable in small scale systems [3].

For the purpose of harvesting energy from mechanical vibration with piezoelectric materials, two possible installation methods were mostly seen. For structure whose surface undertakes significant alternating deformation, the most direct way to harvest energy is to attach piezoelectric patches to the structural surface, as shown in Fig. 1. On the other hand, for the structure whose surface has small deformation, but undergoes significant movement, it is more suitable to install a base excited PEH device to harvest energy. The configuration of a base excited PEH device is shown in Fig. 2. Since the configurations of these two devices are different, their performances on energy harvesting might also be different. It would be interesting that given the same harvesting circuit connected to these two devices, how the different configurations influence the power generation.

To study the dynamics of a PEH device, it is desirable to have a model, which can describe the dynamics of both of its mechanical structure and electrical circuit. Yet, the characteristics of multiple vibration modes on mechanical part and nonlinearity[1] on electrical part obstruct the integration of their models. Up to now, nearly all studies emphasizing on the mechanical part adopted simplified electrical models, e.g., making the real interface circuit equivalent to a linear resistor [4], [5]; while studies emphasizing on the electrical part adopted simplified mechanical models, e.g., neglecting the mechanical dynamics [6], [7]. The majority of researches focused on ei-

[1] For PEH, as far as the target applications are low power electronics, which are usually powered by DC voltage source, an AC-DC conversion is necessary. The AC-DC conversion circuits are all nonlinear.

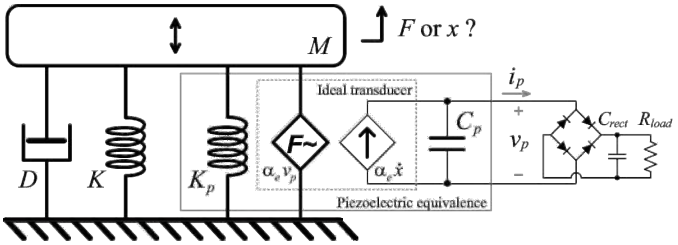

Fig. 3. SDOF representation of a general PEH device.

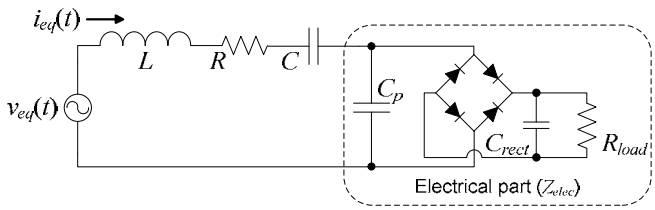

Fig. 4. Equivalent circuit of a PEH device.

ther mechanical or electrical parts, but not both. Liang and Liao proposed the impedance based analysis to PEH devices [8]. Based on some assumptions, all components in both the mechanical and electrical parts of a PEH device are represented by their equivalent impedances. This impedance uniform enables the analytical study on the dynamics of the overall system. Moreover, the energy flow within the PEH system can be quantitatively obtained with the impedance based analysis.

In this paper, the principles on the impedance based analysis in PEH are introduced in Section II. Based on these fundamentals, the harvesting performances of the above-mentioned PEH configurations are investigated in Section III. Experimental and analytical results are compared in Section IV. At the end, a conclusion is given in Section V.

II. Principles

A. Piezoelectric Energy Harvesting

Fig. 3 shows the single degree-of-freedom (SDOF) schematic representation of a general PEH device. The dynamics of this SDOF representation is described by the following equations

$$\begin{cases} M\ddot{x}(t)+D\dot{x}(t)+\left(K+K_p\right)x(t)+\alpha_e v_p(t)=F(t) \\ i_p(t)=\alpha_e\dot{x}(t)-C_p\dot{v}_p(t) \end{cases}. \quad (1)$$

M, D, K, and K_p are the mass, mechanical damping (dissipation), structural stiffness, and piezoelectric short circuit stiffness in the mechanical domain; F and x represent the applied force and displacement of the mass, respectively. $_e$ is the force-voltage coupling factor of the piezoelectric element. Because of the vibration, alternating deformation is produced in the piezoelectric element. With the electromechanical coupling characteristics, it induces a periodic charge flow through the element. A standard energy harvesting (SEH) interface circuit is connected to collect the converted electrical energy. SEH is the most standard interface for AC-DC rectification. The accumulated charge is stored in the filter capacitor C_{rect}, so as to deliver DC power to the load resistor R_{load}. In the electrical domain, C_p is piezoelectric clamped capacitance. v_p and i_p represent the voltage across and current through the piezoelectric element, respectively.

Both the mechanical structure and the electrical circuit influence the performance on power generation. However, their correlation was not profoundly investigated in previous studies.

Sophisticated mechanical configurations were proposed to broaden the harvesting bandwidth [9], increase the transduction coefficient [10], etc. In these studies that were emphasized on mechanical structures, the harvesting circuit was usually simplified by making equivalent to a linear resistor. On the other hand, some literatures stressed the role of the harvesting circuit. The harvesting power could be maximized by tuning the rectified voltage in SEH [6]. Moreover, the harvesting power can be further increased by implementing some sophisticated interface circuits, e.g., synchronized switching harvesting on inductor (SSHI) [7]. In these studies that were emphasized on harvesting circuits, the effect of the mechanical part was simplified as a current source, while the mechanical dynamics was not fully considered.

B. Equivalent Circuit

In the research of PEH, equivalent circuit is one of the most investigated techniques to model the dynamics of a PEH device [11] - [13]. For the PEH device shown in Fig. 3, taking the mechanical to electrical analogy, the force and velocity are equivalent to voltage and current with the following relations

$$v_{eq}(t)=\frac{F(t)}{\alpha_e}, \qquad i_{eq}(t)=\alpha_e\dot{x}(t); \quad (2)$$

while the mass, mechanical damping, and stiffness are equivalent to inductance, resistance, and capacitance with the relations of

$$L=\frac{M}{\alpha_e^2}, \qquad R=\frac{D}{\alpha_e^2}, \qquad C=\frac{\alpha_e^2}{K+K_p}. \quad (3)$$

Fig. 4 gives the equivalent circuit of the PEH device as shown in Fig. 3. With the equivalent circuit, the dynamics of the whole system can be discussed in pure electrical domain with some circuit simulation tools [14]. Yet, computational effort and accuracy are two concerns in numerical simulation. It would be time consuming to search for the maximum harvesting power with numerical analysis. Analytical results on the system dynamics as well as power generation are desired, in particular for harvesting power optimization.

C. Equivalent Impedance Network

The maximum power theorem is regarded as theoretical base for load power optimization. In linear circuit, the power delivered to the load is maximized when the load impedance matches the source impedance, i.e., being complex conjugate of the source impedance. Kim et al. [10] and Kong et al. [15] investigated the impedance matching issue by taking the electrical part of the PEH device (composed of C_p and the harvesting circuit connected in parallel) as resistive impedance; while

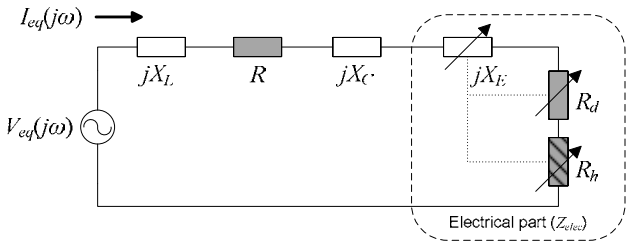

Fig. 5. Equivalent impedance network of a PEH device.

Brufau-Penella and Puig-Vidal investigated the same issue by taking the equivalent impedance as complex conjugate to the source impedance [16]. In the above-mentioned literatures, the definition on the equivalent impedance of a real harvesting circuit, which is nonlinear in nature, was lacked or one-sided. Liang and Liao clarified the definition by studying the fundamental components of the electrical part voltage and current [8]. The equivalent impedance of the electrical part was obtained and denoted as Z_{elec}. Different interface circuits have different available ranges of Z_{elec}. For each interface circuit connected, only the impedance values within the corresponding range are attainable for Z_{elec}.

In addition, within the electrical part, there are three possible branches of energy flow. The energy flowing into the electrical part might be dissipated, harvested, or return to the mechanical part [11]. Taking these three functions into consideration, Z_{elec} is further subdivided into three components: the dissipative component R_d, the harvesting component R_h, and the reactance component X_E [8]. The combination of R_d and R_h is the real part of Z_{elec}; while X_E equals to its imaginary part, i.e.,

$$Z_{elec} = R_d + R_h + jX_E. \tag{4}$$

With this distinction, the equivalent circuit can be further specified as an equivalent impedance network, as shown in Fig. 5.

Different from ordinary impedance, the values of R_d, R_h and X_E are all functions of excitation frequency ω and non-dimensional rectified voltage

$$\tilde{V}_{rect} = \frac{V_{rect}}{V_{OC}}, \tag{5}$$

where V_{OC} is the open circuit voltage given by

$$V_{OC} = \frac{I_{eq}}{\omega C_p} = \frac{\alpha_e X}{C_p}. \tag{6}$$

X denotes the magnitude of the displacement x. Their values are constrained, but variable within the constraints and related with each other.

The power absorbed by R_h corresponds to the harvesting power in a PEH device, which is the target of harvesting power optimization. It is denoted as P_h and calculated with (7). X_L and X_C in (7) are the reactance of L and C, respectively.

III. PEH Devices under Different Excitations

Assuming that the installation of the PEH devices would not change the dynamics of the main structure, the two configurations given in Fig. 1 and Fig. 2 can be modeled as a general PEH device under displacement and force excitations, respectively.

A. Displacement Excitation

The deformation magnitude of the piezoelectric element remains constant under this excitation. According to (2), the magnitude of the equivalent current i_{eq} is also constant when the excitation frequency is fixed. The harvesting power under displacement excitation therefore is given by

$$P_h\left(j\omega, \tilde{V}_{rect}\right) = \frac{I_{eq}^2(j\omega) R_h\left(j\omega, \tilde{V}_{rect}\right)}{2}. \tag{8}$$

The expression on harvesting power is much simpler than that given by (7). Since I_{eq} is not related to $\tilde{V}_{rect}$, with a given excitation frequency, maximum P_h can be obtained when R_h reaches its maximum value.

The value of R_h differs when different interface circuit is connected. In the following parts, the harvesting power in displacement excited PEH devices with three different interface circuits, i.e., SEH, parallel-SSHI (P-SSHI), and series-SSHI (S-SSHI) are compared. The circuit topologies as well as working principles of these interface circuits were introduced in [7] and [17]. The expressions on harvesting power can be obtained by analyzing the energy cycle or work cycle under different interface circuits [11]. The corresponding harvesting components associated with these three interfaces are

$$R_{h,SEH} = \frac{4}{\pi\omega C_p}\left(\tilde{V}_{rect} - \tilde{V}_F\right)\left(1 - \tilde{V}_{rect}\right); \tag{9}$$

$$R_{h,P-SSHI} = \frac{2}{\pi\omega C_p}\left(\tilde{V}_{rect} - \tilde{V}_F\right)\left[2 - \tilde{V}_{rect}(1+\gamma)\right]; \tag{10}$$

$$R_{h,S-SSHI} = \frac{4}{\pi\omega C_p}\frac{1-\gamma}{1+\gamma}\left(\tilde{V}_{rect} - \tilde{V}_F\right)\left(1 - \tilde{V}_{rect}\right), \tag{11}$$

where V_F is the forward voltage drop of the bridge rectifier; $\tilde{V}_F$ is the non-dimensional V_F. γ is the voltage inversion factor during every switching action in SSHI, which was defined in [11]. γ is unchanged once the circuit is built. $R_{h,SEH}$, $R_{h,P\text{-}SSHI}$, and $R_{h,S\text{-}SSHI}$ attain their maxima at

$$P_h\left(j\omega, \tilde{V}_{rect}\right) = \frac{V_{eq}^2(j\omega)}{2} \frac{R_h\left(j\omega, \tilde{V}_{rect}\right)}{\left[X_L(j\omega) + X_C(j\omega) + X_E\left(j\omega, \tilde{V}_{rect}\right)\right]^2 + \left[R + R_d\left(j\omega, \tilde{V}_{rect}\right) + R_h\left(j\omega, \tilde{V}_{rect}\right)\right]^2} \tag{7}$$

$$\frac{\partial\left(2P_h/V_{eq}^2\right)}{\partial\widetilde{V}_{rect}}=\left[\left(X_L+X_C+X_E\right)^2+\left(R+R_d\right)^2-R_h^2\right]\frac{\partial R_h}{\partial\widetilde{V}_{rect}}-2R_h\left(R+R_d+R_h\right)\frac{\partial R_d}{\partial\widetilde{V}_{rect}}-2R_h\left(X_L+X_C+X_E\right)\frac{\partial X_E}{\partial\widetilde{V}_{rect}}=0 \quad (16)$$

$$\left(\widetilde{V}_{rect,opt}\right)_{SEH}=\frac{1-\widetilde{V}_F}{2}; \quad (12)$$

$$\left(\widetilde{V}_{rect,opt}\right)_{P-SSHI}=\frac{1}{1+\gamma}-\frac{\widetilde{V}_F}{2}; \quad (13)$$

$$\left(\widetilde{V}_{rect,opt}\right)_{S-SSHI}=\frac{1-\widetilde{V}_F}{2}. \quad (14)$$

When $V_{OC} >> V_F$, we can neglect the $\widetilde{V}_F$ terms in (12) - (14) and obtain similar results to those proposed in [17]. It should be noted that the previous studies were emphasized on the optimization of the harvesting circuits under displacement excitation. Early literatures treated the piezoelectric structures as a current source in parallel with the piezoelectric capacitance C_p [6]. The implicit assumption of this equivalence is that the displacement magnitude is constant. Recent literatures started their analyses from differential equations, which are similar to (1) [7]. Yet, in these studies, the force magnitude in fact was only used to determine the displacement magnitude at resonant frequency. Other than this, the analyses were all based on displacement excitation.

B. Force Excitation

In the base excitation case, the peak magnitude of the base acceleration, i.e., $\ddot{y}(t)$, remains constant. Given the base displacement $y(t)$ and denoting the relative displacement of the cantilever free end as $x(t)$, the dynamics of the base excited cantilever can be simplified into SDOF representation and described by the following equations

$$\begin{cases} M\ddot{x}(t)+D\dot{x}(t)+\left(K+K_p\right)x(t)+\alpha_e v_p(t)=-M\ddot{y}(t) \\ i_p(t)=\alpha_e\dot{x}(t)-C_p\dot{v}_p(t) \end{cases}. \quad (15)$$

Comparing (1) and (15), and taking $-M\ddot{y}(t)$ as the equivalent force, the base excitation problem therefore is converted into force excitation.

Unlike that in displacement excitation, the dynamics of other components, in both mechanical and electrical parts, influence the vibration displacement, and subsequently affect the harvesting power. As discussed in Section II, (7) gave the expression of harvesting power as a function of ω and $\widetilde{V}_{rect}$ under force excitation. When the excitation frequency ω is determined, maximum P_h is obtained at the zero derivative point, as specified in (16).

The corresponding dissipation and imaginary components in SEH, P-SSHI, and S-SSHI are

$$R_{d,SEH}=\frac{4}{\pi\omega C_p}\widetilde{V}_F\left(1-\widetilde{V}_{rect}\right), \quad (17)$$

$$X_{E,SEH}=\frac{1}{\pi\omega C_p}\left(\sin\theta\cos\theta-\theta\right), \quad (18)$$

$$R_{d,P-SSHI}=\frac{1}{\pi\omega C_p}\left\{2\widetilde{V}_F\left[2-\widetilde{V}_{rect}\left(1+\gamma\right)\right]+\widetilde{V}_{rect}^2\left(1-\gamma^2\right)\right\}, \quad (19)$$

$$X_{E,P-SSHI}=\frac{1}{\pi\omega C_p}\left(\sin\theta\cos\theta-\theta\right), \quad (20)$$

$$R_{d,S-SSHI}=\frac{4}{\pi\omega C_p}\frac{1-\gamma}{1+\gamma}\left(1-\widetilde{V}_{rect}+\widetilde{V}_F\right)\left(1-\widetilde{V}_{rect}\right), \quad (21)$$

$$X_{E,S-SSHI}=-\frac{1}{\omega C_p}, \quad (22)$$

respectively. θ is the rectifier blocked phase in a half cycle. It is linked with $\widetilde{V}_{rect}$ with the relation of [2]

$$\cos\theta=1-\left(1+\gamma\right)\widetilde{V}_{rect}. \quad (23)$$

Theoretically, for the SEH case, optimum $\widetilde{V}_{rect}$ is obtainable by substituting (9), (17), and (18) into (16), then solving the equation (similarly, for the P-SSHI case, substituting (10), (19), and (20); for the S-SSHI case, substituting (11), (21), and (22)). Close form expressions on optimum $\widetilde{V}_{rect}$, which are similar to (12) - (14) under displacement excitation, are preferred; however, the transcendental equation is unable to be solved with analytical method. It is solvable with numerical method; it seems more convenient to obtain the optimum $\widetilde{V}_{rect}$ by substituting the expressions of R_h, R_d, and X_E into (7) and numerically searching for the maximum P_h.

C. Comparison

The parameters of an experimental PEH device, which will be introduced in Section IV, are given in TABLE I. Based on these parameters; the harvesting powers with three interface circuits under two excitations are investigated. Fig. 6 shows the contours of harvesting power P_h as well as the corresponding optimum $\widetilde{V}_{rect}$ in six cases.

For displacement excitation, the magnitude of open circuit V_{OC} under different excitation frequency maintains at 8.4 V. With the relation given in (6), the displacement magnitude of the equivalent mass is 0.92 mm. It can be observed from Fig. 6 (a), (c), and (e) that the optimum $\widetilde{V}_{rect}$ in all SEH, P-SSHI, and S-SSHI cases is constant under displacement excitation, in spite of the frequency difference. The optimum $\widetilde{V}_{rect}$ under displacement excitation is located at the middle of the harvestable range (light gray in Fig. 6) of $\widetilde{V}_{rect}$, which is also expressed in (12) - (14) .

[2] SEH can be regarded as a particular case of P-SSHI, in which the inversion factor =1.

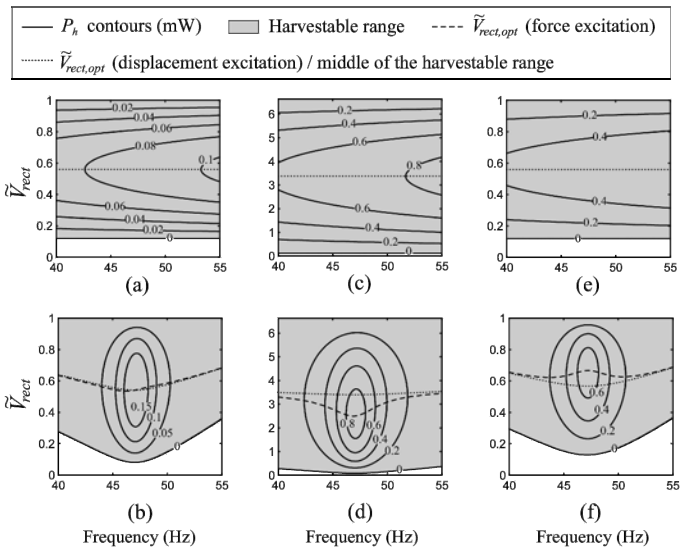

Fig. 6. Contours of harvesting power P_h.
(a) SEH, displacement excitation. (b) SEH, force excitation.
(c) P-SSHI, displacement excitation. (d) P-SSHI, force excitation.
(e) S-SSHI, displacement excitation. (f) S-SSHI, force excitation.

For force (base) excitation, the applied acceleration to the base excited piezoelectric cantilever is 10 m/s^2 in RMS value. As observed from Fig. 6 (b), (d), and (f), the optimum $\widetilde{V}_{rect}$ varies with excitation frequency in the three cases. Lefeuvre et al. regarded the optimum $\widetilde{V}_{rect}$ under force excitation (shown by dash curves in Fig. 6) the same as that under displacement excitation, i.e., the middle points of the harvestable range (shown by dot curves) [7]; yet, it is shown in these figures that they are in fact different, in particular, the difference gets larger around the resonant frequency.

IV. Experiment

A. Experimental Setup

Fig. 7 shows the experimental setup. The main mechanical structure is an aluminum cantilever, whose excitation is from a shaker (4810, B & K). A piezoceramic patch of 49mm x 24mm x 0.508mm (T120-A4E-602, Piezo System, Inc.) is bonded near the fixed end, where the lognitudinal deformation of the piezoelectric element is generated according to the transverse vibration of the cantilever. An accelerometer (4501, B & K) is installed at the fixed end to track the base acceleration. For the purpose of synchronization in both P-SSHI and S-SSHI, an electromagnetic sensor is employed to sense the relative velocity between the cantilever beam and the base. The permanent magnet acts as proof mass at the same time. It can lower the vibration frequency and increase the displacement of the free end. The output voltage from the coil, which is proportional to the end velocity, is then input to a micro-controller unit (eZ430-RF2500, Texas Instrument). In the circuitry part, the micro-controller is coded to firstly analyze the velocity signal, and then generate switching command to drive the MOSFET switch to perform synchronized switching actions. TABLE I gives the

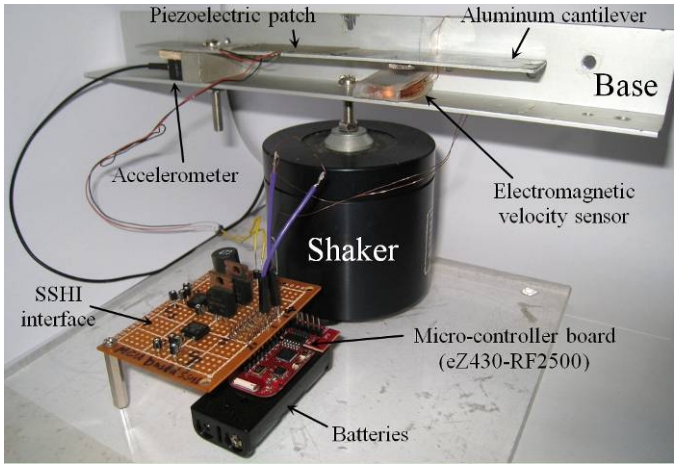

Fig. 7. Experimental setup.

TABLE I
Parameters of the Experimental Setup

Parameter	Value
α_e	3.12*10^{-4} N/V
f_0	47.09 Hz
sw	MOSFET (IRL510)
Rectifier	DB104 (V_F = 1.0V)
γ	- 0.7
L_i	47 mH
C_{rect}	1, 10, 22 μF
C_p	34.40 nF
L	40.7 kH
C	280.67 pF
R	1 MΩ

parameters of the experimental setup, including mechanical structure and interface circuit.

The equivalent impedance of the mechanical part is obtained with experimental identification. Without excitation applied and shunt circuit connected, the internal impedance of the piezoelectric structure can be obtained by fitting the frequency response waveforms measured by an impedance analyzer (4294A, Agilent). The component values of L, C, R, and C_p are also listed in TABLE I.

The relative displacement of the cantilever as well as the base acceleration might drift under different harvesting conditions. As long as the relative velocity is related with the relative displacement, to perform constant displacement excitation, the electromagnetic sensor is used to sense the relative velocity of the cantilever and then adjust the excitation signal for maintaining same displacement magnitude under different situations. For constant force excitation, it is adjusted by referring to the output of the accelerometer.

B. Results

For any interface circuit connected, the harvesting power under different $\widetilde{V}_{rect}$ can be experimentally obtained by connecting different DC load resistor R_{load} to the storage capacitor C_{rect}. The corresponding rectified voltage is the voltage across R_{load} plus V_F, the harvested power delivered to R_{load} is

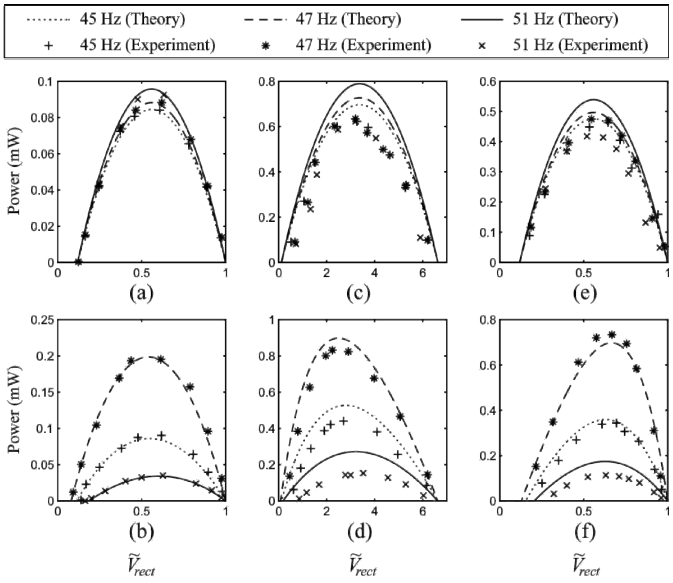

Fig. 8. Theoretical and experimental harvesting power with three different interface circuits under two excitations, respectively.
(a) SEH, displacement excitation. (b) SEH, force excitation.
(c) P-SSHI, displacement excitation. (d) P-SSHI, force excitation.
(e) S-SSHI, displacement excitation. (f) S-SSHI, force excitation.

$$P_{h,exp} = \frac{\left(V_{rect} - V_F\right)^2}{R_{load}}. \tag{24}$$

Fig. 8 summarized the theoretical and experimental results under three excitation frequencies near the resonant frequency in six cases (connecting with three interface circuits, under two excitations, respectively). The theoretical results agree with the experimental data quite well. We now compare the results of those two groups under different excitations. Under force excitation, the harvesting power declines significantly when the excitation frequency is away from the resonant frequency. While under displacement excitation, the changes in harvesting power are not significant for small frequency drift. In terms of the shape of a single curve under a specified excitation frequency, in displacement excitation, it is symmetric; while in force excitation, it is asymmetric.

V. Conclusion

Different from the models given in the previous literatures, which oversimplified either the electrical or mechanical part, the impedance based analysis provided a methodology to uniformly model both the mechanical and electrical parts in a piezoelectric energy harvesting (PEH) device. It can be utilized to study the overall dynamics as well as the harvesting performance of a PEH system. Two installations of PEH devices were discussed. Each of them should be adopted according to different vibration conditions of the substrate structure. The two configurations can be modeled as a general PEH device under two excitation manners, i.e., displacement and force excitations. The difference between those two excitations was discussed. Their performances in energy harvesting, in terms of harvesting power, were analyzed with the impedance based method. In particular, this method can accurately show how the harvesting performance is influenced by the system dynamics under different excitation frequencies, which was never done in the previous studies.

Acknowledgment

The work described in this paper was supported by the grant from Research Grants Council (Project No. CUHK 414809) of Hong Kong Special Administrative Region, China.

References

[1] J. Paradiso and T. Starner, “Energy scavenging for mobile and wireless electronics,” *IEEE Pervasive Comput.*, vol. 4, no. 1, pp. 18–27, 2005.

[2] S. R. Anton and H. A. Sodano, “A review of power harvesting using piezoelectric materials (2003-2006),” *Smart Mater. Struct.*, vol. 16, no. 3, pp. R1-R21, 2007.

[3] S. P. Beeby, M. J. Tudor, and N. M. White, “Energy harvesting vibration sources for microsystems applications,” *Meas. Sci. Tech.*, vol. 17, pp. R175-R195, 2006.

[4] A. Erturk and D. Inman, “On mechanical modeling of cantilevered piezoelectric vibration energy harvesters,” *J. Intell. Mater. Syst. Struct.*, vol. 19, pp. 1311-1325, 2008.

[5] M. Zhu, E. Worthington, and J. Njuguna, “Analyses of power output of piezoelectric energy-harvesting devices directly connected to a load resistor using a coupled piezoelectric-circuit finite element method,” *IEEE Trans. Ultras. Ferro. Freq.*, vol. 56, pp. 1309-1317, 2009.

[6] G. Ottman, H. Hofmann, A. Bhatt, and G. Lesieutre, “Adaptive piezoelectric energy harvesting circuit for wireless remote power supply,” *IEEE Trans. Power Elec.*, vol. 17, no. 5, pp. 669-676, Sep 2002.

[7] E. Lefeuvre, A. Badel, C. Richard, L. Petit, and D. Guyomar, “A comparison between several vibration-powered piezoelectric generators for standalone systems,” *Sens. Actuator A-Phys.*, vol. 126, no. 2, pp. 405-416, 2006.

[8] J. Liang and W. H. Liao, "Impedance matching for improving piezoelectric energy harvesting systems," *Proceedings of SPIE Smart Structures/NDE conferences*, March 7-11, 2010.

[9] A. Erturk, J. M. Renno, and D. J. Inman, “Modeling of piezoelectric energy harvesting from an l-shaped beam-mass structure with an application to UAVs,” *J. Intell. Mater. Syst. Struct.*, vol. 20, pp. 529-544, 2009.

[10] H. Kim, S. Priya, H. Stephanou, and K. Uchino, “Consideration of impedance matching techniques for efficient piezoelectric energy harvesting,” *IEEE Trans. Ultras. Ferro. Freq.*, vol. 54, pp. 1851-1859, 2007.

[11] J. R. Liang and W. H. Liao, “Piezoelectric energy harvesting and dissipation on structural damping,” *J. Intell. Mater. Syst. Struct.*, vol. 20, pp. 515-527, 2009.

[12] N. G. Elvin and A. A. Elvin, “A general equivalent circuit model for piezoelectric generators,” *J. Intell. Mater. Syst. Struct.*, vol. 20, pp. 3-9, 2009.

[13] Y. Yang and L. Tang, “Equivalent circuit modeling of piezoelectric energy harvesters,” *J. Intell. Mater. Syst. Struct.*, vol. 20, pp. 2223-2235, 2009.

[14] Y. C. Shu, I. C. Lien, and W. J. Wu, “An improved analysis of the SSHI interface in piezoelectric energy harvesting,” *Smart Mater. Struct.*, vol. 16, pp. 2253-2264, 2007.

[15] N. Kong, D. S. Ha, A. Erturk, and D. J. Inman, “Resistive impedance matching circuit for piezoelectric energy harvesting,” *J. Intell. Mater. Syst. Struct.* (*OnlineFirst*), 1045389X0935797, 2010.

[16] J. Brufau-Penella and M. Puig-Vidal, “Piezoelectric energy harvesting improvement with complex conjugate impedance matching,” *J. Intell. Mater. Syst. Struct.*,, vol. 20, pp. 597-608, 2009.

[17] A. Badel, A. Benayad, E. Lefeuvre, L. Lebrun, C. Richard, and D. Guyomar, “Single crystals and nonlinear process for outstanding vibration-powered electrical generators,” *IEEE Trans. Ultras. Ferro. Freq.*, vol. 53, pp. 673-684, 2006.